富山大学水素同位体機能研究センター研究報告15：65－74，1995

論　文

ガス・プラズマ駆動による水素透過フラックスの一般式

舒　　衛民・渡辺国昭

富山大学水素同位体機能研究センター
〒930　富山市五福3190

A General Formula for Simultaneous Plasma- and Gas-Driven Hydrogen Permeation

W. M. SHU and Kuniaki WATANABE

Hydrogen Isotope Research Center, Toyama University, Toyama 930, Japan
(Received September 29, 1995 ; accepted December 22, 1995)

Abstract

A general formula for simultaneous plasma- and gas-driven permeation has been developed using the electrical analog approach, in which the permeation potential and resistance are defined for both diffusion in the bulk and recombination on the surface. This formula is used to calculate the permeation flux of deuterium through 316 stainles steel. The theory agreed very well with the experimental results of Doyle and Brice. The dependencies of permeation flux on gas pressure, incident flux, thickness of membrane, ratio of recombination coefficients, ratio of diffusion coefficients and ratio of solubility coefficients on both sides, are also discussed.

1. Introduction

A complete understanding of hydrogen transport is important for characterizing materials used in the components which are directly exposed to the hydrogen isotope plasma confined in a tokamak. The analysis of hydrogen transport through plasma facing materials, therefore, has been carried out so far by many research groups. Waelbrock et al. developed a single transport parameter to describe the hydrogen permeation flux (Φ_p) and recycle flux, and focused on gas-driven permeation (GDP)[1, 2].

Doyle and Brice derived formalism to describe steady-state hydrogen transport in materials exposed to hydrogen gas and/or plasma[3-5]. Nagasaki et al. modified the formalism of Doyle and Brice by focusing on the ion-induced increment in the concentration and the permeation flux of hydrogen rather than the total ones[6,7]. Shu et al. developed new coupled parameters to distinguish the regimes of plasma-driven permeation (PDP)[8,9], and derived the general formulae of Φ_p in GDP and PDP by an electrical analog[10].

The analytical descriptions, although approximations, have a few clear advantages over the numerical solutions[11]. First they are easy to use and can therefore provide a guide in selecting parameters for the calculations. Secondly, and more importantly, the analytical formulation allows new physical insight into the functional dependencies and interrelationships among the plasma and material parameters.

The permeation flux, Φ_p of hydrogen through a membrane should be determined from bulk properties and surface parameters of materials as well as the experimental conditions. However, the expression for Φ_p was only available for two specific cases in GDP[12,13] and four specific cases in PDP[6-8]. The existing models have almost focused on distinguishing the specific regimes[1-9]. However, it is much more crucial to determine the expression for Φ_p in general case. Shu et al.[10] developed an electrical analog approach which brought about a general solution for Φ_p in GDP and PDP. In this work, the analog approach is applied to simultaneous plasma- and gas-driven permeation to obtain a general formula for Φ_p. The formula is applied to calculate the permeation flux of deuterium through 316 stainless steel for varying parameters, such as gas pressure, incident flux, thickness of membrane, ratio of recombination coefficients, ratio of diffusion coefficients and ratio of solubility coefficients on both sides. This will lead to better understanding and new physical insight into the actual permeation phenomena.

2. Analog model for simultaneous plasma- and gas-driven permeation

Details of the electrical approach were described elsewhere[10]. For a laminate membrane in which each layer is normal to a flow, new parameters are defined for the resistances per unit area to diffusion on the front and back sides, γ and α, and to recombination on the both sides, ρ_f and ρ_f, as :

$$\gamma \equiv \frac{r}{D_f S_f}, \quad \alpha \equiv \sum_{j=1}^{n} \frac{L_j}{D_j S_j}, \quad \rho_b \equiv \frac{1}{S_b \sqrt{k_b \Phi_b}} = \frac{\beta_b}{\sqrt{\Phi_b}} \quad \text{and} \quad \rho_f \equiv \frac{1}{S_f \sqrt{k_f \Phi_f}} = \frac{\beta_f}{\sqrt{\Phi_f}},$$

where r is the implanted range, L_j, D_j and S_j are the thickness, diffusion coefficient and solubility coefficient for the jth ($j=1, 2, 3...n$) lamina, respectively, k_f and k_b are recombination coefficients on the front and back sides, S_f and S_b are solubility coefficients in the first lamina and final lamina, D_f is diffusion coefficient in the first lamina, Φ_b and Φ_f are fluxes through the back and front surfaces.

The permeation circuit of simultaneous plasma- and gas-driven permeation in steady state is schematically shown in Fig. 1. It contains two hydrogen sources (ε_P and ε_G) and a parallel connection of the resistors on the front side ($\gamma + \rho_f$) and those on the back side ($\alpha + \rho_b$). P and Φ_i in Fig. 1 are hydrogen pressure and incident flux.

According to the principle of superposition, the permeation flux to the back side, Φ_p, is given by

$$\Phi_p = \Phi_p^G + \Phi_p^p, \tag{1}$$

where Φ_p^G is the flux of gas-driven permeation, and Φ_p^p is that of plasma-driven permeation.

On the assumption that $\gamma + \rho_f \ll \alpha + \rho_b$, Φ_p is given as

$$\Phi_p = \frac{\varepsilon_G + \varepsilon_P}{\alpha + \rho_b} = \frac{\sqrt{P} + \gamma\,\Phi_i + \beta_f\sqrt{\Phi_i}}{\alpha + \beta / \sqrt{\Phi_p}}. \tag{2}$$

Therefore, the permeation flux for simultaneous plasma- and gas-driven permeation is obtained as

$$\Phi_p = \frac{4\,(\sqrt{P} + \gamma\,\Phi_i + \beta_f\sqrt{\Phi_i})^2}{(\beta_b + \sqrt{\beta_b^2 + 4\,\alpha\,(\sqrt{P} + \gamma\,\Phi_i + \beta_f\sqrt{\Phi_i})})^2}. \tag{3}$$

From this equation, the permeation flux for the following two specific cases is easily derived.

(1) When $\sqrt{P} \gg \gamma\,\Phi_i + \beta_f\sqrt{\Phi_i}$, it becomes gas-driven permeation ; Eq. 3 is simplified to Eq. 4,

$$\Phi_p = \frac{4P}{(\beta_b + \sqrt{\beta_b^2 + 4\,\alpha\sqrt{P}})^2}. \tag{4}$$

At large enough pressure, that is $P \gg \frac{\beta_b^4}{\alpha^2}$, permeation flux is obtained as $\Phi_p = \frac{\sqrt{P}}{\alpha}$.

At small enough pressure, that is $P \ll \frac{\beta_b^4}{\alpha^2}$, permeation flux is obtained as $\Phi_p = \frac{P}{\beta_b^2}$.

(2) When $\sqrt{P} \ll \gamma\,\Phi_i + \beta_f\sqrt{\Phi_i}$, it becomes plasma-driven permeation ; Eq. 3 is simplified to Eq. 5

$$\Phi_P = \frac{4\ (\gamma\ \Phi_i + \beta_f\sqrt{\Phi_i})^2}{(\beta_b + \sqrt{\beta_b^2 + 4\ \alpha\ (\gamma\ \Phi_i + \beta_f\sqrt{\Phi_i})})^2}\ . \tag{5}$$

On the basis of the comparisons between the permeation resistance for recombination (R) and that for diffusion (D) on each side, Φ_P in four specific categories of PDP can be identified. 1) The RR regime, that is $\rho_f \gg \gamma$ and $\rho_b \ll \alpha$; permeation flux is obtained as $\Phi_P = \frac{\beta_f^2}{\beta_b^2}\Phi_i$. 2) The RD regime, that is $\rho_f \gg \gamma$ and $\alpha \gg \rho_b$; permeation flux is obtained as $\Phi_P = \frac{\beta_f}{\alpha}\sqrt{\Phi_i}$. 3) The DD regime, that is $\gamma \gg \rho_f$ and $\alpha \gg \rho_b$; permeation flux is obtained as $\Phi_P = \frac{\gamma}{\alpha}\Phi_i$. 4) The DR regime, that is $\gamma \gg \rho_f$ and $\rho_b \gg \alpha$; permeation flux is obtained as $\Phi_P = \frac{\gamma^2}{\beta_b^2}\Phi_i^2$.

The permeation flux, Φ_P, in four specific regimes of PDP is summarized in Table 1.

Table 1. Φ_P in four specific regimes of PDP through a single laminate.

Regime	RR	RD	DD	DR
Φ_P	$\frac{\beta_f^2}{\beta_b^2}\Phi_i$	$\frac{\beta_f}{\alpha}\sqrt{\Phi}$	$\frac{\gamma}{\alpha}\Phi_i$	$\frac{\gamma^2}{\beta_b^2}\Phi_i^2$

When $n=1$, and $S_f=S_b$, the expressions for Φ_P in Table 1, can be simplified to the existing ones[6-8].

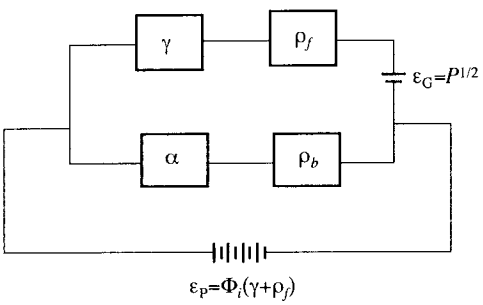

Fig. 1 Schematic representation of the permeation circuit for simultaneous plasma- and gas-driven permeation in steady state.

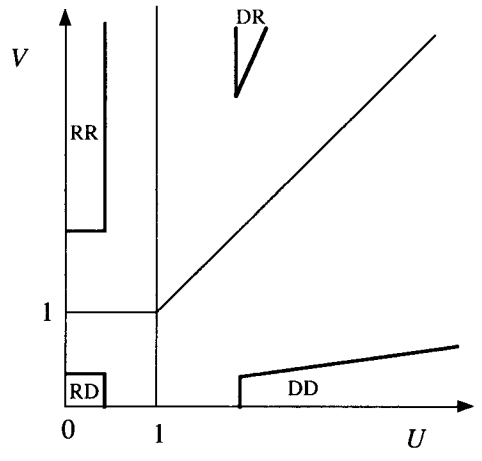

Fig. 2 Four specific regimes of PDP distinguished by coupled parameters, U and V.

In order to distinguish the four regimes, two normalized parameters, U and V, are defined as $U \equiv \frac{\gamma \sqrt{\Phi_i}}{\beta_f}$ and $V \equiv \frac{\beta_b{}^2}{\alpha \beta \sqrt{\Phi_i}}$.

As shown in Fig. 2, the specific four regimes in plasma-driven permeation can be distinguished using the coupled parameters, U and V. For the RR regime, $U \ll 1$ and $V \gg 1$; for the RD regime, $U \ll 1$ and $V \ll 1$; for the DD regime, $U \gg 1$ and $U/V \gg 1$; for the DR regime, $U \gg 1$ and $U/V \ll 1$. It is also shown in Fig. 2 that only for the four specific areas, the permeation flux Φ_P can be calculated from Table 1. For other areas in Fig. 2, Φ_P must be calculated by the general formula (Eq. 5).

3. Application to 316 stainless steel

An application of the general formula to permeation flux of deuterium through 316 stainless steel is shown in Fig. 3. The points labeled with a open square in this figure are the experimental results of Doyle and Brice under the conditions *of* $P=2.8$ Pa, $L=4\ \mu$m, r=400 Å and $\Phi_i = 3.1 \times 10^{19}$ atoms/m^{2}s[14]. The curves for "GAS +PLASMA", "GAS ALONE" and "PLASMA ALONE" in Fig. 3 are calculated with Eqs. 3, 4 and 5, respectively. The following input data are used in the calculations :

$$D = D_f = D_b = 4.7 \times 10^{-7} e^{-6500/T} \quad \text{m}^2/\text{s}, \tag{6}$$

$$k_b = 1.5 \times 10^{-23} e^{-11600/T} \quad \text{m}^4/\text{s}, \tag{7}$$

$$k_f = 3000 k_b \tag{8}$$

and

$$S = S_f = S_b = 2.2 \times 10^{23} e^{-696/T} \quad \text{atoms/m}^3/\text{Pa}^{1/2}, \tag{9}$$

where the diffusivity and solubility were taken from Louthan and Derrick[15] and the recombination coefficients on both sides were from Doyle and Brice[14].

It can be seen in Fig. 3 that the formula for simultaneous plasma- and gas-driven permeation (Eq. 3) agrees very well with the experimental results. Both results calculated for "GAS ALONE" (Eq. 4) and "PLASMA ALONE" (Eq. 5) approximately follow two straight lines on this Arrhenius plot. As temperature increases, the former increases rapidly, whereas the latter decreases gradually. Below 500 K, plasma-driven permeation dominates the permeation flux. In other words, Eq. 5 is the asymptotic solution of Eq. 3 for low temperature. Above 1000 K, on the other hand, plasma-driven permeation can be neglected, and Eq. 4 is the asymptotic solution of Eq. 3 for high temperature.

Eq. 3 shows that the permeation flux depends upon hydrogen sources (P and Φ_i), permeation resistors on the front side ($\gamma + \rho_f$) and those on the back side ($\alpha + \rho_b$). On the front side, ($\gamma + \rho_f$) is a function of incident range, r, diffusivity, D_f, solubility coefficient, S_f, and recombination coefficient, k_f. On the back side, for single layer case, ($\alpha + \rho_b$) is a function of the thickness of the membrane, L, diffusivity, D_b, solubility coefficient, S_b, and recombination coefficient, k_b.

According to Eq. 3, the permeation flux of hydrogen through 316 stainless steel is calculated with varying parameters, such as gas pressure, incident flux, thickness of membrane, ratio of recombination coefficients, ratio of diffusion coefficients and ratio of solubility coefficients on both sides. In the calculation, only one parameter is changed, other data are the same as those of Doyle and Brice. The results calculated are shown in Fig. 4 to 9, which are Arrhenius plots of the permeation flux as a function of inverse temperature.

As shown in Fig. 4, the permeation flux of hydrogen through 316 stainless steel increases more rapidly with increasing hydrogen pressure at higher temperatures. At temperatures lower than 500 K, permeation flux changes little with varying pressure. This indicates that gas-driven permeation plays dominant role at higher temperatures for this case. On the other hand, it is shown in Fig. 5 that as incident flux increases, the permeation flux of hydrogen through 316 stainless steel increases much mor rapidly at lower temperatures. At temperatures higher than 900 K, permeation flux changes little with varying incident flux. This also suggests that plasma-driven permeation plays dominant role at lower temperatures.

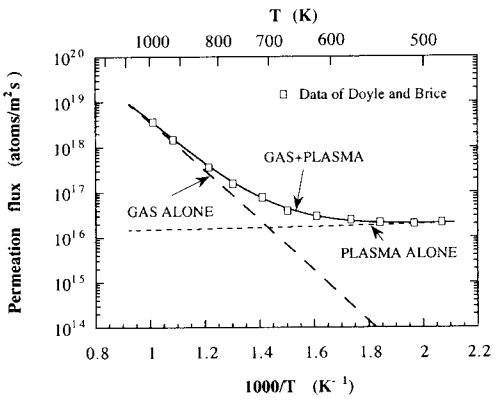

Fig. 3 Comparison between calculated and experimental results of permeation flux for 316 stainless steel.

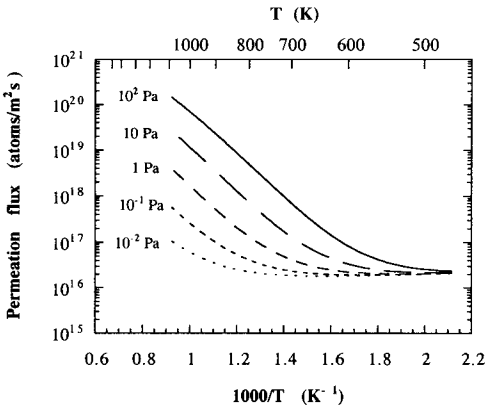

Fig. 4 Arrhenius plot of permeation flux as a function of inverse temperature for varying hydrogen pressure.

Because both gas-driven and plasma-driven permeations depend on the thickness of the membrane, the permeation flux decreases with increasing thickness at all temperatures, as shown in Fig. 6. It is also noticeable that there is no much difference between the data of 10^{-5} m and those of 10^{-6} m below about 700 K. This suggests that the permeation resistance for diffusion becomes much smaller than that for recombination when thickness is smaller than 10^{-5} m and temperature lower than 700 K.

Many experimental results[16-18] have shown that the recombination coefficient on the front side, k_f, may be three or four orders of magnitude greater than the recombination coefficient on the back side, k_b, and that k_f continuously increases during the first implantation for a few cases, for instance after leaving the membran in a vacuum overnight. The calculation of permeation flux for varying ratio of k_f/k_b is shown in Fig. 7. The permeation flux decreases rapidly with increasing k_f/k_b below 700 K, but changes little when $k_f/k_b > 10^3$ and $T > 900$ K, where diffusion becomes rate-limiting factor.

Two possibilities have been proposed for the variation of diffusion coefficient D_f, on the front side. One is the reduction of diffusion by the hydrogen trapping sites produced during irradiation[19]. Another is the enhanced diffusion by the formation of short path (self interstitial atoms) at temperatures lower than 700 K[20]. The calculation of permeation flux for varying D_f/D_b has been performed from 10^{-2} to 10^2. It can be seen in Fig. 8 that permeation flux decreases rapidly with increasing D_f/D_b when $D_f/D_b < 10$ and $T < 700$ K, but there appears no difference between $D_f/D_b = 10$ and $D_f/D_b = 10^2$. It suggests that recombination becomes rate-limiting

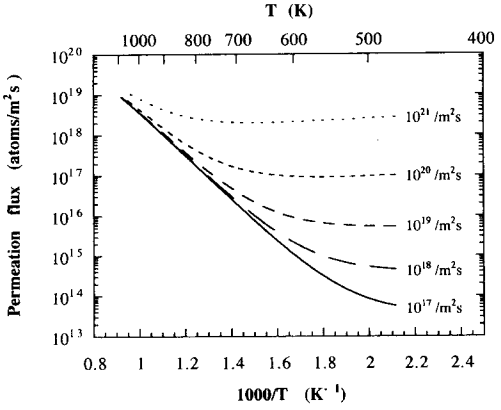

Fig. 5 Arrhenius plot of permeation flux as a function of inverse temperature for varying incident flux.

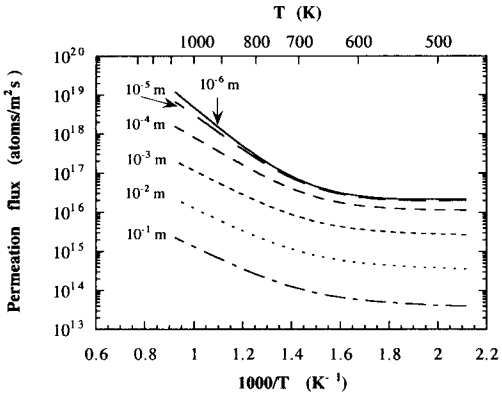

Fig. 6 Arrhenius plot of permeation flux as a function of inverse temperature for varying membrane thickness.

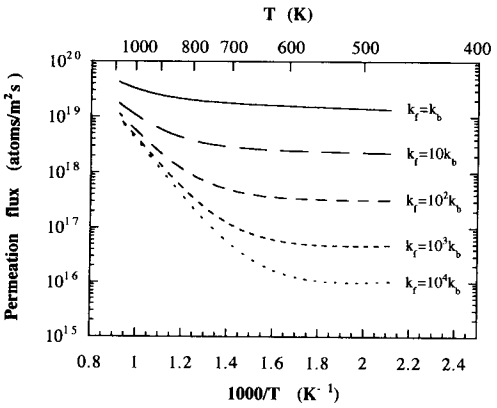

Fig. 7 Arrhenius plot of permeation flux as a function of inverse temperature for varying k_f/k_b.

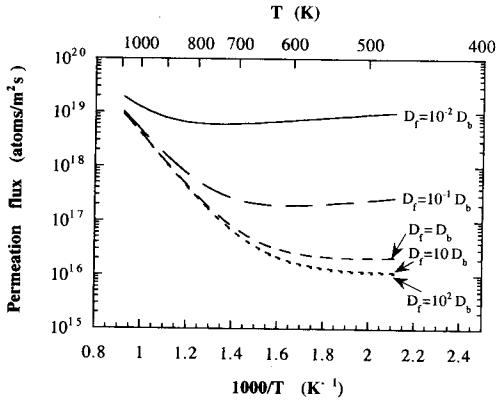

Fig. 8 Arrhenius plot of permeation flux as a function of inverse temperature for varying D_f/D_b.

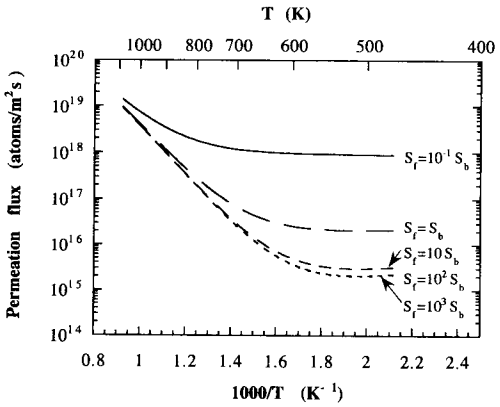

Fig. 9 Arrhenius plot of permeation flux as a function of inverse temperature for varying S_f/S_b.

factor if $D_f/D_b>10$.

The permeation resistance for both diffusion and recombination depends on the solubility coefficient. However, the effect of irradiation on the solubility on the front side, S_f, has not been investigated yet. The calculation of permeation flux for varying S_f/S_b was performed from 10^{-1} to 10^3 and shown in Fig. 9. The permeation flux decreases rapidly with increasing S_f/S_b when $S_f/S_b<10$ and $T<600$ K, but there seems no difference for $S_f/S_b=10^2$ and $S_f/S_b=10^3$. This indicates that permeation flux through 316 stainless steel is independent on S_f/S_b when $S_f/S_b>10^2$.

4. Conclusions

(1) By the analog approach, the general expression of Φ_p for simultaneous plasma- and gas-driven permeation in steady state is obtained as

$$\Phi_P=\frac{4\ (\sqrt{P}+\gamma\ \Phi_i+\beta\sqrt{\Phi_i})^2}{(\beta_b+\sqrt{\beta_b^2+4\ \alpha\ (\sqrt{P}+\gamma\ \Phi_i+\beta\sqrt{\Phi_i})})^2}\ .$$

(2) The general formula agrees very well with the experimental results of Doyle and Brice.

(3) When $\sqrt{P} \gg \gamma \Phi_i + \beta_f \sqrt{\Phi_i}$, only gas-driven permeation can be considered. On the other hand, if $\sqrt{P} \ll \gamma \Phi_i + \beta_f \sqrt{\Phi_i}$ only plasma-driven permeation can be taken into account.

(4) The general expression of Φ_P gives a simple way to examine the dependencies of permeation flux upon hydrogen pressure, incident flux, sample size, implanted range, recombination coefficients on both sides, diffusion coefficients on both sides and solubility coefficients on both sides.

References

1) F.Waelbroeck, P.Wienhold, J.Winter, E.Rota and T.Banno, Kerenforschungsanlage, Julich, Germany, Rep. No. Jul, (1984) 1966.

2) F.Waelbroeck, P.Wienhold, J.Winter, J.Nucl. Mater., **111-112** (1982) 185.

3) B.L.Doyle, J.Nucl. Mater., **111-112** (1982) 628.

4) B.L.Doyle and D.K.Brice, Radiat. Eff., **89** (1985) 21.

5) D.K.Brice and B.L.Doyle, J.Vac., Sci. Technol., **A 5** (1987) 2311.

6) T.Nagasaki, R.Yamada, M.Saidoh and H.Katsuta, J.Nucl. Mater., **151** (1988) 189.

7) T.Nagasaki and H.Ohno, J.Vac. Sci. Technol., **A 11** (1993) 588.

8) W.M.Shu, K.Okuno and Y.Hayashi, J.Phys. Chem., **97** (1993) 4497.

9) W.M.Shu, Y.Hayashi and K.Okuno, Phil. Mag., **B 72** (1995) 301.

10) W.M.Shu, Y.Hayashi and M.Sugisaki, Acta Metall., (1996).

11) P.Wienhold, I.Ali-Kahn, K.J.Dietz, M.Profant and F.Waelbrock, J.Nucl. Mater., **86-87** (1979) 1001.

12) A.A.Haasz, P.L.Andrew and A.B.Antoniazzi, J.Vac., Sci. Technol., **A 7** (1989) 1042.

13) P.L.Andrew and A.A.Haasz, J.Less-common Metals, **172-174** (1991) 732.

14) B.L.Doyle and D.K.Brice, J.Nucl. Mater., **145-147** (1987) 288.

15) M.R.Louthan and D.G.Derrick, Corrosion Sci., **15** (1975) 565.

16) A.I.Livshits, M.E.Notkin and A.A.Samartsev, J.Nucl. Mater., **170** (1990) 79.

17) W.M.Shu, K.Okuno, Y.Hayashi and Y.Naruse, J.Nucl. Mater., **203** (1993) 55.

18) W.M.Shu, Y.Hayashi and K.Okuno, J.Alloys Compounds, **193** (1993) 213.

19) W.M.Shu, K.Okuno, Y.Hayashi, S.Ohira and Y.Naruse, Fusion Technol., **21** (1992) 1934.

20) R.A.Kerst and W.A.Swansiger, J.Nucl. Mater., **122-123** (1984) 1499.

APPENDIX

Nomenclature

Φ_P permeation flux (atoms/m^{2}s)

r implanted range (m)

D_f diffusion coefficient in the first lamina (m^2/s)

S_f solubility coefficient in the first lamina (atoms/m^3/Pa$^{1/2}$)

γ resistance for diffusion on the front side (m^{2}sPa$^{1/2}$/atoms)

L_j thickness for the jth (j=1, 2, 3...n) lamina (m)

D_j diffusion coefficient for the jth (j=1, 2, 3...n) lamina (m^2/s)

S_j solubility coefficient for the jth (j=1, 2, 3...n) lamina (atoms/m^3/Pa$^{1/2}$)

α total resistance in the bulk to permeation through a unit area (m^{2}sPa$^{1/2}$/atoms)

S_b solubility coefficient in the final lamina (atoms/m^3/Pa$^{1/2}$)

k_b recombination coefficient on the back side (m^4/s/atoms)

Φ_b permeation flux through the back surface (atoms/m^{2}s)

β_b function of bulk property S_b and surface parameter k_b (ms$^{1/2}$Pa$^{1/2}$/atoms$^{1/2}$)

ρ_b permeation resistance per unit area of the back surface (m^{2}sPa$^{1/2}$/atoms)

S_f solubility coefficient in the first lamina (atoms/m^3/Pa$^{1/2}$)

k_f recombination coefficient on the front side (m^4/s/atoms)

Φ_f permeation flux through the front surface (atoms/m^{2}s)

β_f function of bulk property S_f and surface parameter k_f (ms$^{1/2}$Pa$^{1/2}$/atoms$^{1/2}$)

ρ_f permeation resistance per unit area of the front surface (m^{2}sPa$^{1/2}$/atoms)

P upstream hydrogen pressure (Pa)

ε_G hydrogen source of gas-driven permeation (Pa$^{1/2}$)

ε_P hydrogen source of plsama-driven permeation (Pa$^{1/2}$)

Φ_P^G permeation flux driven by gas (atoms/m^{2}s)

Φ_P^P permeation flux driven by plasma (atoms/m^{2}s)

U normalized transport parameter

V normalized transport parameter